Supporting Information

Paramagnetic CuS Hollow Nanoflowers for T_2–FLAIR Magnetic Resonance Imaging-guided Thermochemotherapy of Cancer

Hao Zhang [a,b,†], Yaodong Chen [c,†], Yunyu Cai [a,*], Jun Liu [a], Pengfei Liu [d], Zizhuo Li [c], Tingting An [c], Xiuhua Yang [c,*], and Changhao Liang [a,b,*]

(Hao Zhang and Yaodong Chen contributed equally to this work.)

[a] *Key Laboratory of Materials Physics and Anhui Key Laboratory of Nanomaterials and Nanotechnology, Institute of Solid State Physics, Hefei Institutes of Physical Science, Chinese Academy of Sciences, Hefei 230031, Anhui, China*

[b] *Department of Materials Science and Engineering, University of Science and Technology of China, Hefei, 230026, China*

[c] *Department of Abdominal Ultrasound, The First Affiliated Hospital of Harbin Medical University, Harbin 150001, China*

[d] *Department of Magnetic Resonance, The First Affiliated Hospital of Harbin Medical University, Harbin 150001, China*

* Corresponding author E-mail: hydyyyxh@163.com, chliang@issp.ac.cn, yycai@issp.ac.cn

† These authors contributed equally to this work.

Calculation of the photothermal conversion efficiency

Temperature of the sample was recorded during the cooling period for the calculation of photothermal conversion efficiency (η). First, a total of 0.5 mL of CuS HNs dispersion (100 μg/mL) was added to a quartz cuvette and irradiated by NIR laser (1064 nm, 3W/cm^2). After the solution reached an equilibrium temperature, the laser was turn off. Then, the system temperature was cooled down to the ambient temperature. According to the calculation method reported by previous literature,[1-2] η of CuS HNs was determined by equation below.

$$\eta = \frac{hS(T_{max} - T_{surr}) - Q_S}{I(1 - 10^{-A_\lambda})} \quad (1)$$

Where T_{max} is the maximum temperature of the sample, T_{surr} is the surrounding temperature, I is the laser power, A_λ is the absorbance of the sample at the excitation wavelength (λ), h is the heat transfer coefficient of the sample system, S is the surface area of the container.

The equation (1) is based on the total energy balance of system:

$$\Sigma_i m_i C_{pi} \frac{dT}{dt} = Q_{NPs} + Q_S - Q_{loss} \quad (2)$$

where m, C_p and T are the mass, heat capacity of solvent and solution temperature, respectively.

Q_{NPs} is the phototheraml energy input by CuS HNs and can be calculated by equation (3):

$$Q_{NPs} = I(1 - 10^{-A_\lambda})\eta \quad (3)$$

Q_S is the rate of solvent heat input without the CuS HNs, which was independently measured to be 32.2 mW using pure water.

Q_{loss} is the thermal energy lost to the surroundings:

$$Q_{loss} = hS(T_{max} - T_{surr}) \quad (4)$$

The hS can be defined to equation (5):

$$hS = \frac{mC_{H_2O}}{\tau_s} \quad (5)$$

where m is the mass of the system, C_{H_2O} is the specific heat capacity of water (~ 4.2J/(g·°C)), τ_s is the system time constant of the sample. τ_s was calculated by the equation (6):

$$t = -\tau_s ln\theta = -\tau_s ln\left(\frac{T - T_{surr}}{T_{max} - T_{surr}}\right) \quad (6)$$

The τ_s can be calculated according to the slope of linear time data (t) from the cooling period vs. -ln(θ).

Based on equation (2), the energy input is equal to the energy lost at equilibrium temperature.

$$Q_{NPs} + Q_S = Q_{loss} = hS(T_{max} - T_{surr}) \quad (7)$$

Thus, η of CuS HNs can be calculated according to equation (1), equation (5) and equation (6). In our system, the laser power (I) is 0.6 W. For 100 μg/mL CuS HNs dispersion, the absorbance (A_{1064}), evaluated temperature (T_{max}-T_{surr}), and the time constant (τ_s) are 2.13, 22.5 °C, and 224.4 s. Finally, η of CuS HNs was calculated to be 30%.

Calculation of DOX loading capacity

The DOX loading capacity was calculated according to equation:

$$DOX\ loading\ capacity = \frac{Loading\ DOX}{CuS + Loading\ DOX} \times 100\% \quad (1)$$

DOX shows a clear characteristic absorbance peak at about 480 nm in UV-vis spectra. The absorbance value of DOX solution was proportional to its concentration. Then the content of DOX could be estimated according to intensity of its characteristic peak, as following:

$$m_{DOX} = V*n*(1-A_1/A_0) \quad (2)$$

where m_{DOX} is the mass of DOX, V is the DOX solution volume, n is the solution concentration, A_1 and A_0 are the absorbance value of characteristic peak of supernatant solution and initial solution, respectively.

For drug loading experiment, 5 mg of CuS HNs were dispersed in DOX aqueous solution (10 mL, 50 μg/mL) and stirred at room temperature overnight. The characteristic peak was settled at 500 nm,

which will be explained by next answer. As shown in Fig. S3d, the absorbance value of initial DOX and supernatant were 0.948 and 0.686, respectively. Thus m_{DOX} was calculated to be 0.138 mg. Finally, the DOX loading capacity could be calculated to be 2.69%.

Formation mechanism of CuS HNs

In order to reveal the formation mechanism of CuS HNs, samples at each growth stage were characterized. According to our previous work[3], ZnO NPs were prepared and showed a spherical morphology with average diameter of 77 nm in **Fig. S1**a. After the irradiation of ZnO NPs mixed with $Cu(NO_3)_2$ solution via 355 nm pulse laser, ZnO@CuO seed core-shell structure (**Fig. S1**b) was formed. The CuO seeds exhibited a needle-like morphology. When ZnO NPs were irradiated by UV light laser, the photogenerated electrons of ZnO NPs reacted with H_2O to generate OH^- or dissolved O_2 to consume H^+. The elevated pH value around ZnO NPs induced the formation of $[Cu(OH)_4]^{2-}$ clusters as the precursor for the *in situ* formation of CuO on the surface of ZnO NPs.[4-6] Notably, CuO is a p-type semiconductor. A p-n junction, formed at the interface between ZnO and CuO, hindered the transformation of photogenerated electrons to the surface and inhibited the growth of CuO seed. Thus, the surface of ZnO NPs was covered by CuO seeds totally. After the solution was transferred to a dry oven, the CuO HNs were formed through cation ion-exchange reactions between excess Cu ions and ZnO (**Fig. S1**c). Finally, CuS HNs were obtained inheriting the structure of CuO HNs through anion ion-exchange reactions between $(NH_4)_2S$ and CuO (**Fig. S1**d).

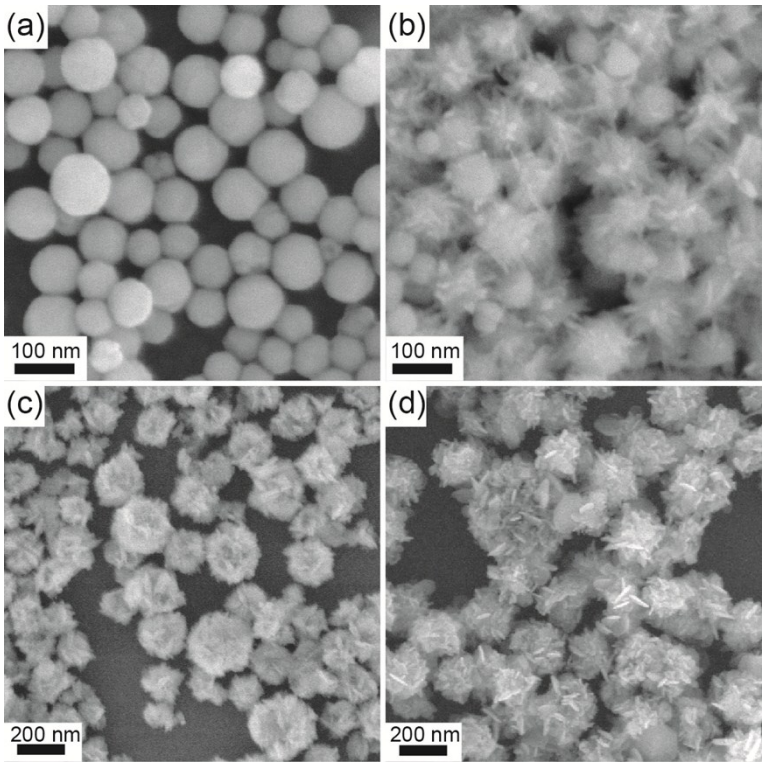

Fig. S1. SEM images of (a) ZnO nanoparticles, (b) ZnO@CuO seed nanoparticles, (c) CuO hollow nanoflowers, and (d) CuS hollow nanoflowers.

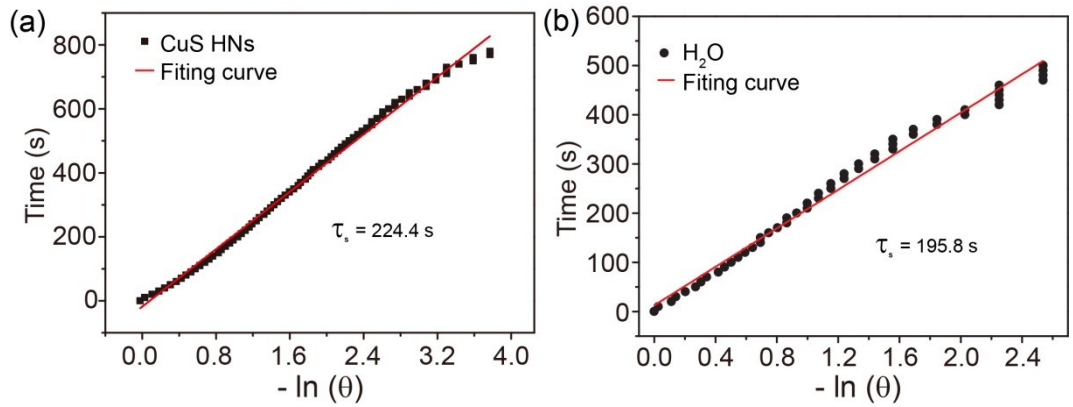

Fig. S2. Plot of cooling time of versus negative natural logarithm of the temperature driving force. Curves of (a) CuS HNs and (b) H_2O, respectively.

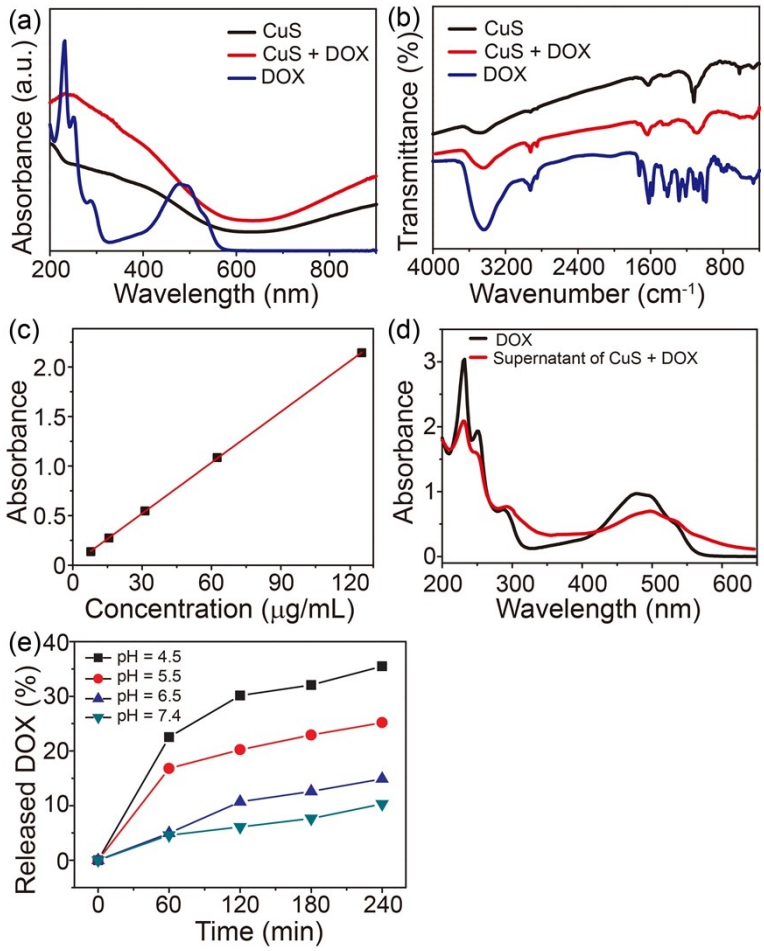

Fig. S3. (a) UV-vis-NIR absorption and (b) FTIR spectra of DOX, CuS HNs, and CuS + DOX. (c) Absorbance of various DOX concentrations at 480 nm. (d) UV-vis-NIR absorption of 50 μg/mL DOX and the supernatant of the mixture containing CuS HNs and DOX. (e) DOX release from the CuS + DOX without laser irradiation at various pH and selected time points.

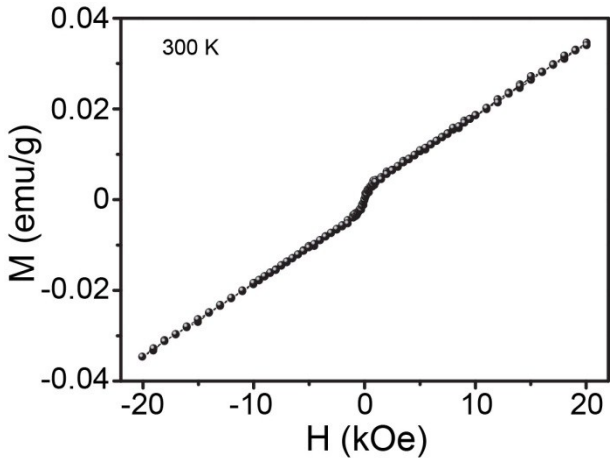

Fig. S4. Hysteresis loop of CuS HNs at 300K.

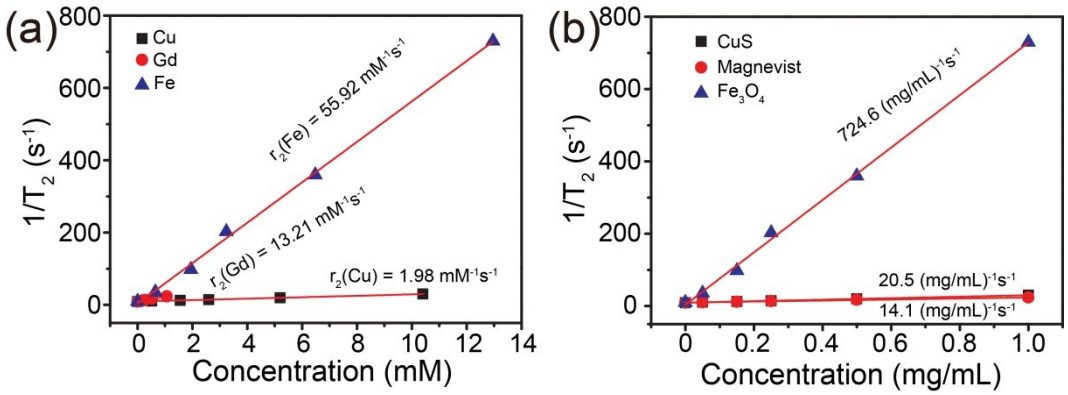

Fig. S5. Linear fittings of $1/T_2$ of CuS HNs, magnevist, and Fe_3O_4 at different (a) Cu, Gd, and Fe concentrations and (b) mass concentrations, respectively.

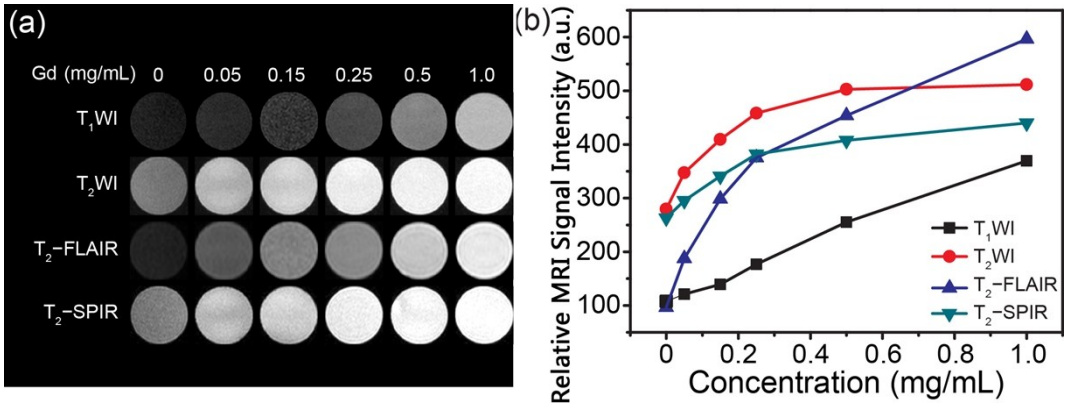

Fig. S6. (a) In vitro MR images of magnevist at different mass concentrations on T_1WI, T_2WI, T_2–FLAIR, and T_2–SPIR sequences, respectively, and (b) the corresponding relative MRI signal intensities.

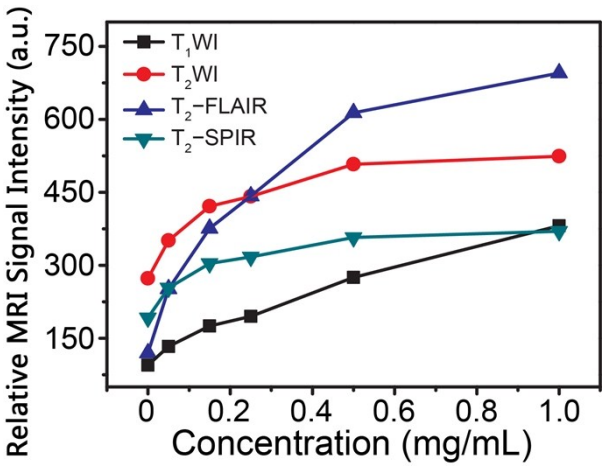

Fig. S7. Relative MRI signal intensity of CuS + DOX aqueous dispersions at different CuS concentrations in T_1WI, T_2WI, T_2–FLAIR, and T_2−SPIR MRI.

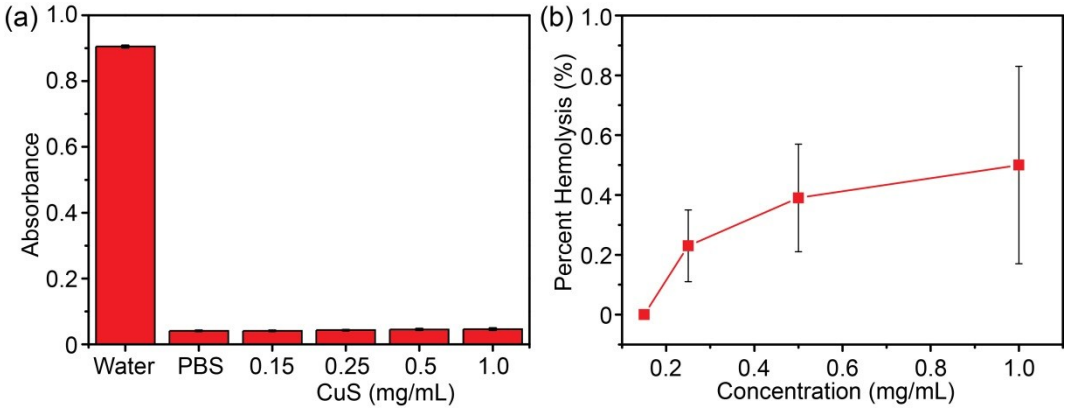

Fig. S8. Hemolytical activity of CuS + DOX. Water and PBS were used as negative and positive controls, respectively. (a) Absorbance values of the supernatants at 570 nm measured by multidetection microplate reader. (b) Hemolytic percent of red blood cells incubated with the CuS + DOX at various concentrations of CuS for 4 h.

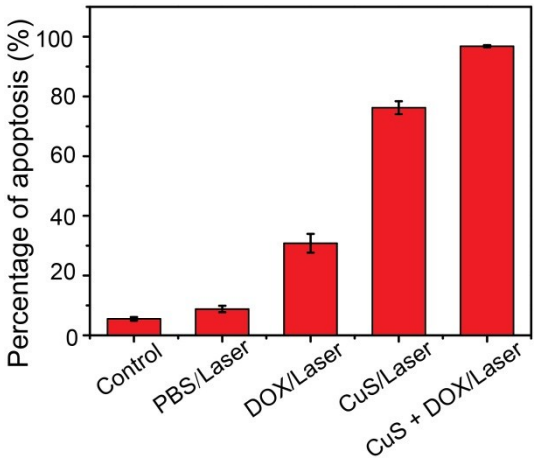

Fig. S9. Percentage of apoptosis in control, PBS/Laser, DOX/Laser, CuS/Laser, and CuS + DOX/Laser group, respectively.

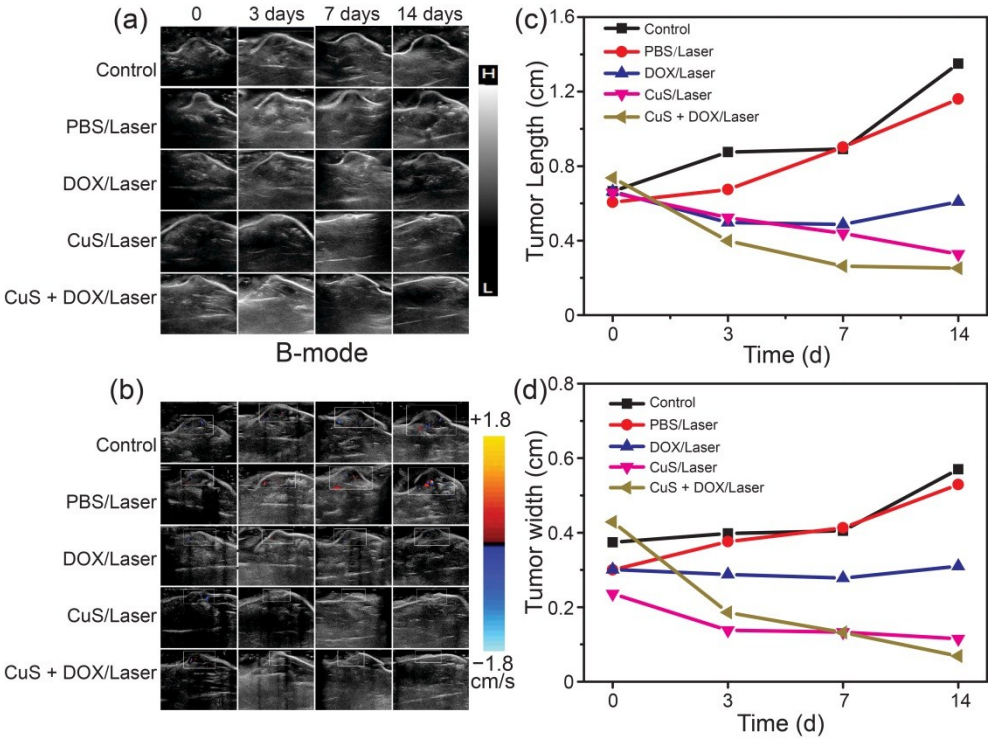

Fig. S10. (a) B-mode ultrasonography and (b) color Doppler flow imaging (CDFI) for monitoring evolution of tumors after treatment. Tumor growth curves in different groups according to B-mode sonogram, including (c) tumor length and (d) tumor width.

References

[1] Z. C. Wu, W. P. Li, C. H. Luo, C. H. Su, C. S. Yeh, *Adv. Funct. Mater.* **2015**, *25*, 6527.

[2] Z. L. Li, J. Liu, Y. Hu, K. A. Howard, Z. Li, X. L. Fan, M. L. Chang, Y. Sun, F. Besenbacher, C. Y. Chen, M. Yu, *ACS Nano* **2016**, *10*, 9646.

[3] H. Zhang, S. L. Wu, J. Liu, Y. Y. Cai, C. H. Liang, *Phys. Chem. Chem. Phys.* **2016**, *18*, 22503.

[4] J. Kim, W. Kim, K. Yong, *J. Phys. Chem. C* **2012**, *116*, 15682.

[5] S. Jung, S. Jeon, K. Yong, *Nanotechnology* **2011**, *22* 015606.

[6] Y. Cudennec, A. Lecerf, *Solid State Sci.* **2003**, *5*, 1471.